RSC Advances

This is an *Accepted Manuscript*, which has been through the Royal Society of Chemistry peer review process and has been accepted for publication.

Accepted Manuscripts are published online shortly after acceptance, before technical editing, formatting and proof reading. Using this free service, authors can make their results available to the community, in citable form, before we publish the edited article. This *Accepted Manuscript* will be replaced by the edited, formatted and paginated article as soon as this is available.

You can find more information about *Accepted Manuscripts* in the Information for Authors.

Please note that technical editing may introduce minor changes to the text and/or graphics, which may alter content. The journal's standard Terms & Conditions and the Ethical guidelines still apply. In no event shall the Royal Society of Chemistry be held responsible for any errors or omissions in this *Accepted Manuscript* or any consequences arising from the use of any information it contains.

ROYAL SOCIETY OF CHEMISTRY

www.rsc.org/advances

Probing the correlation between structure, carrier dynamics and defect states of epitaxial GaN film on $(11\bar{2}0)$ sapphire grown by rf-molecular beam epitaxy

Shibin Krishna T C[a†], Neha Aggarwal[a†], G. Anurag Reddy[a†], Palak Dugar[a], Monu Mishra[a†], Lalit Goswami[a], Nita Dilawar[b], Mahesh Kumar[a], K K Maurya[c] and Govind Gupta[a †*]

[a]Physics of Energy Harvesting Division, CSIR-National Physical Laboratory, Dr K S Krishnan Road, New Delhi-110012, India
[b]Apex Level Standards & Industrial Metrology, CSIR-National Physical Laboratory, Dr K S Krishnan Road, New Delhi-110012, India
[c]Sophisticated and Analytical Instrumentation, CSIR-National Physical Laboratory, Dr. K.S. Krishnan Road, New Delhi-110012, India
[†]Academy of Science & Innovative Research (AcSIR), CSIR-NPL Campus, Dr. K.S. Krishnan Road, New Delhi-110012, India

** Corresponding author: E-mail address: govind@nplindia.org*
Tel.: +91-11-45608403, Fax: +91-11-4560-9310

Received (in XXX, XXX) XthXXXXXXXXX 20XX, Accepted Xth XXXXXXXXX 20XX
DOI: 10.1039/b000000x

A systematic study has been performed to correlate structural, optical and electrical properties with defect states in the GaN films grown on a-plane $(11\bar{2}0)$ Sapphire substrate via rf-plasma molecular beam epitaxy. Morphological analysis reveals the presence of small lateral size (30-70 nm) hexagonally shaped V- pits on the GaN films. These V-defects possibly contribute as the main source of non-radiative decay. High resolution X-ray diffraction reveals highly single crystalline GaN film grown on a-plane sapphire substrate where the threading dislocations are the cause of V-defects in the GaN film. Photoluminescence measurement shows a highly luminescence band to band emission of GaN film at 3.41 eV along with a broad defect band emission centered at 2.2 eV. A detailed optical and electrical analysis has been carried out to study the defects states and related carrier dynamics for determining the efficacy of the film for device fabrication. The variation in the low temperature current voltage measurements confirms the presence of deep level defects in mid- band gap region while transient spectroscopy shows that non radiative decay is the dominant relaxation mechanism for the photo excited-carriers from these defect states.

1. Introduction

Group-III nitride based semiconductors have shown marked potential to serve as the basis of new generation of optoelectronic, high-temperature and high-power microelectronic devices[1,2]. These materials are generally grown heteroepitaxially on foreign substrates like Al_2O_3, SiC, Si etc[3], since it is difficult to grow GaN single crystals and GaN templates are still not cost-effective. The advances in the growth technologies have significantly improved the crystal quality of epitaxial layers, however large difference in the lattice constants and thermal expansion coefficients between epitaxial layer and the substrate still remains a problem. The search for a suitable substrate to grow good quality epitaxial GaN films has been mainly directed towards study of c-plane (0001) sapphire[3]. Several approaches have been adapted to optimize the nucleation and growth of epitaxial GaN to overcome the large mismatch in lattice (14%) and thermal expansion coefficient (56%). The growth of GaN on c-plane sapphire is hindered by high density of various crystallographic defects such as dislocations and domain boundaries etc[4]. In contrast, there are reports in literatures using a-plane sapphire substrate as a replacement for c-plane sapphire substrate since the lattice mismatches being 1.8% and−0.62% for [0002] GaN parallel to [11-20] sapphire and [1-100] GaN parallel to [1-100] sapphire respectively[5]. Lower lattice mismatch will lead to the growth of GaN with better crystalline quality, lesser defects and hence better devices. Moustakas et. al. have shown that GaN films grown on a-plane sapphire with initial nitridation and low temperature GaN buffer layers lead to smooth surface morphology compared to those grown on c-plane sapphire[6,7]. In addition to smooth surface morphology and crystalline quality which are prerequisite for device-competent semiconductor material, it is also imperative that we take into account the influence of trap states, centers for radiative and non-radiative recombination in the material. There have also been some studies on the effect of GaN and AlN buffer layers on the growth of GaN on a-plane sapphire[8]. Few groups have reported a comparative study on the performance of InGaN/AlGaN multiple quantum well LEDs grown on a-plane and c-plane sapphire substrates[9,10]. It was found that LEDs grown on a-plane sapphire substrates showed superior optoelectronic and crystalline properties as compared to the ones grown under identical conditions on c-plane sapphire substrates: decreased x-ray diffraction line width, reduced pit density, and smaller ideality factor. However, there has not been any extensive study of GaN grown on a-plane sapphire substrate from the point of view of device fabrication. Thus, it is important to investigate the structural and optical properties of GaN film grown on a-plane sapphire substrate which can lead to the development of comprehensive understanding into the high quality epitaxially grown GaN film.

RSC Advances Accepted Manuscript

In the present work, we have demonstrated highly crystalline quality of the epitaxially grown GaN film on a-plane sapphire substrate and the structural and optical properties have been studied and explored in detail. Additionally, from the perspective of device fabrication, the influence of defects on device performance should be considered too. Therefore, the generated defects states and related dynamics are explored and incorporated through I-V and Transient Spectroscopy.

2. Experimental

2.1 Growth of GaN

GaN growth on $(11\bar{2}0)$ sapphire substrate was carried out using RIBER Compact 21 PAMBE system equipped with standard Riber Pyrolytic Boron Nitride (PBN) effusion cells and a plasma source (ADDON RF-plasma source) to supply active nitrogen (N^*) species. The a-plane sapphire substrate was chemically pre-cleaned by using the standard cleaning procedure followed by out-gassing in the buffer chamber at 600 °C. Nitridation of substrate was performed at low substrate temperature (450°C). A LT-GaN buffer layer was deposited at 530 °C under Ga-rich conditions. The epitaxial GaN film was grown for 150 minutes at rf plasma power of 500 W which has a growth rate of 3 nm/min (Ga beam equivalent pressure (BEP) of 9E-7 Torr) at 735 °C. Fig 1 (a) shows the schematic cross sectional view of grown layers on a-plane sapphire substrate. The growth was monitored in-situ by reflection high energy electron diffraction (RHEED) using STAIB electron gun (12 keV) to ensure high quality two-dimensional (2D) growth. The growth temperature was monitored by optical pyrometer (error value of ±5 °C) calibrated with thermocouple.

2.2 Characterization

The analysis of the growth structure and crystalline nature of GaN film was carried out by High Resolution X-Ray Diffraction (HRXRD, Panalytical X'Pert PRO MRD System) instrument using Cu K_α radiation (λ= 1.5405Å) with a scan rate of 0.05°/sec and slit width of 0.1mm. Field Emission Secondary Electron Microscopy (FESEM, ZEISS AURIGA) equipment was employed to characterize the morphological properties of grown GaN film. The optical properties of the grown film have been investigated by performing photoluminescence (PL) spectroscopy using a He–Cd laser operating at 325 nm as an excitation source. Micro-Raman measurements were performed using Horiba T 64000 Raman triple spectrometer equipped with an excitation source of Argon ion laser (Ar+) operating at a wavelength of 514 nm with a power of 50 mW and a charge coupled device system having an accuracy of 0.5 cm^{-1} to collect the scattered data. The electrical properties of the grown film were analyzed by I-V measurements. Prior to loading the samples in an evaporation chamber for depositing metal contacts, standard cleaning procedure was followed. Each sample was cleaned using acetone, methanol and isopropanol in that order to remove organic, inorganic and physical impurities such as dust or excessive moisture. The wafers were then dried using pressurized nitrogen. Au was deposited by Physical Vapor Deposition (PVD) for contacts formation. Femtosecond transient absorption spectroscopy has been performed by a setup comprising of an oscillator (Micra), amplifier (Coherent Legend), Optical Parametric Amplifier, OPA (TOPAS) and the spectroscopy system (Helios, Ultrafast Systems). The 4 mJ (1 KHz) output of the amplifier with a pulse width of 35 fs centered at 800 nm is split to two parts. One of the parts is fed to the OPA with 1.8 mJ energy and the other part 0.5 mJ is fed to the spectrometer via a delay stage of 0-8 ns. The pulse width after passing through TOPAS is about 70 fs. The broad band white light has been generated inside the spectrometer by passing the spitted beam through sapphire cylindrical crystal, which is capable of generating probe pulse in the range of 450-850 nm. A highly stable 320 nm of the OPA output has been selected as a pump beam and the fluence was fixed at 40 μJ/cm^2. The fitting of the data is done with the help of Surface Xplorer analysis software.

3. Results and discussion

A crystallographic model of the cross-sectional view of the interface of GaN and the a-plane sapphire substrate is shown in Fig 1 (b). It is clearly see that GaN growth on a- plane sapphire implies the epitaxial orientation relationship of (0001) GaN//$(11\bar{2}0)$ sapphire, which is consistent with our experimental RHEED observations described below. In Fig. 1 (b), the top monolayer of ''O'' atoms in sapphire have been replaced by ''N'' atoms. It is known that the sapphire lattice is terminated by oxygen atoms at the surface[11]. This presence of oxygen species at the interface can complicate the epitaxy of GaN, by formation of Ga-O layer at the interface hence the a-plane sapphire is exposed to nitrogen plasma resulting in the replacement of all the O atoms on the surface by N atoms, thereby forming a monolayer of strained AlN. This facilitates the subsequent growth of GaN on a better chemically matched substrate.

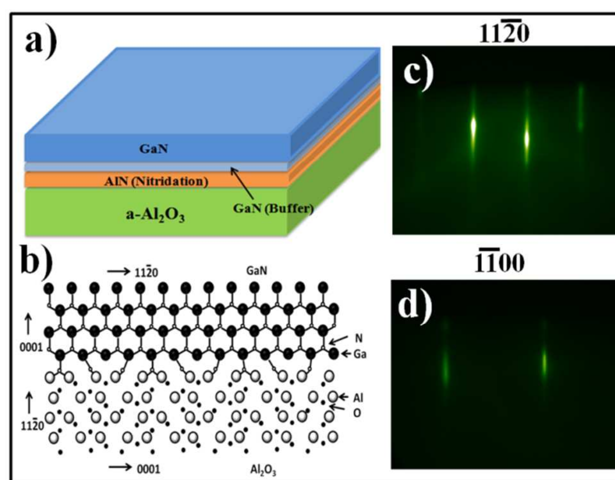

Figure 1: a) Schematic diagram of the individually stacked layers on a-plane sapphire substrate, b) crystallographic model of cross-sectional view of the GaN and a- plane sapphire interface. Real time RHEED patterns observed along the $(11\bar{2}0)$ *and* $(1\bar{1}00)$ *zone axis for GaN (c,d).*

The RHEED pattern observed for GaN along $(11\bar{2}0)$ and $(1\bar{1}00)$ zone axes are shown in Fig 1 (c,d). The sharp streaky typical 1x1 reconstructed RHEED pattern of GaN film has been observed. The kikuchi diffraction pattern observed along $(11\bar{2}0)$ direction illustrates the two-dimensional (2D) growth of GaN epitaxial film with high crystalline quality. The camera length of the diffraction system was calculated and used to estimate the interplanar spacing of the planes responsible for the pattern. Based on these calculations, it was confirmed that GaN growth on a-plane sapphire has the epitaxial orientation relationship of (0001) GaN//$(11\bar{2}0)$ sapphire. Therefore, high crystalline quality

RSC Advances Accepted Manuscript

wurtzite structure GaN film is grown epitaxially along c-direction on a-plane sapphire substrate.

The surface morphology of the grown GaN film was examined by using FESEM. Fig. 2 (a) exhibits the large area FESEM image of the GaN film on a-plane sapphire substrate. The surface of the film was continuous and hexagonal shaped pits with variable size distribution. Inset Fig. 2 (a) shows zoomed area FESEM image to clearly visualize the pit shape & size. The average pits density was calculated to be 6.7E8 cm^{-2} and variation in the lateral size of the hexagonal shaped pits is found to be between 30 nm to 70 nm. These pits are in the form of V-defects on the GaN surface[12,13]. The threading dislocations (TD) with different core energies[14,15] are responsible for different sizes of V-defects on the surface. The formation of V-pits could result from the strain relaxation between GaN film and the substrate. A schematic representation of V-defects mediated hexagonal pits is shown in Fig. 2 (b). These V defects have an open hexagonal, inverted pyramid with $(10\bar{1}1)$ and $(1\bar{1}01)$ are the adjacent hexagonal side walls[16]. Many researchers have reported that for heteroepitaxy, there is always a TD connected with the bottom of V defect and the cause of V-defect formation is the increased strain energy[17,18]. Recently Kim et.al.[19] reported the phenomenon included the correlation of carrier recombination and lateral V-defects size. Small lateral size of V-pits leads to lateral diffusion of carriers which suggests more non-radiative recombination domains. Hence, we propose that the small lateral size (30-70 nm) of the V- pits on the GaN film grown on a- plane sapphire could lead to large non-radiative recombination of carriers. The carrier dynamics relating to the presence of defect states and their recombinations are explored in detailed in subsequent section (transient spectroscopy analysis). Figure 2 (c) shows the cross sectional FESEM image of GaN/a-sapphire. A sharp heterostructure interface has been observed and the thickness was found to be 440 nm.

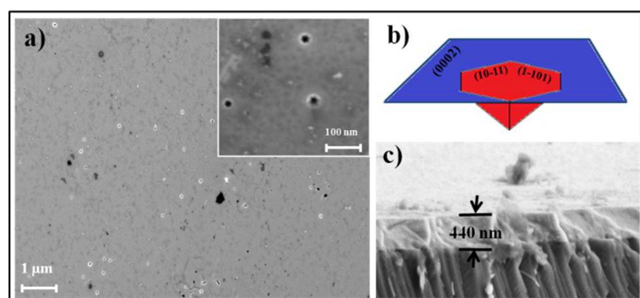

Figure 2: a) FESEM image of GaN film grown on a-plane sapphire substrate b) schematic representation of hexagonal pits on the GaN surface c) cross sectional FESEM image of GaN/a-sapphire.

A more detailed structural analysis and study of crystalline quality of the grown film has been explained through HRXRD analysis. Fig. 3(a) shows a 2Θ-ω scan of GaN film grown on a-plane sapphire substrate. The 2-theta peak positions at 34.67° and 72.95° are attributed to diffraction along (0002) and (0004) plane of GaN respectively. The (0002) plane diffraction angle of heteroepitaxial GaN was close to that of strain free bulk GaN (34.57°)[20] which might be due to the lattice relaxation of the GaN film grown on a less lattice mismatched (~2% along c-direction) a-plane sapphire substrate. In addition, two sharp peaks at 2-theta position of 37.9° and 80. 85° are ascribed to $(11\bar{2}0)$ and $(22\bar{4}0)$ plane of diffraction from a-sapphire substrate. The apparent presence of first and second order x-ray diffractions of GaN in the 2 theta-omega scan illustrates the highly crystalline GaN film grown along the c-direction epitaxially on a-plane sapphire substrate. The lattice constants in the growth direction (along c-axis) for GaN is calculated directly by using Bragg's law,

$$2d_{hkl} \sin\theta_{hkl} = n.\lambda \qquad (1)$$

where, d is the lattice spacing, which is given by $d_{hkl} = 1/ \sqrt{\{ [(4/3)*\{(h^2 + hk + k^2)/a\}^2] + (l/c)^2 \}}$ for hexagonal symmetry system, θ is the measured angle of diffraction, hkl are the miller indices, λ is the wavelength of x-ray source ($CuK_{\alpha 1}$= 1.5406 Å) and 'a' & 'c' are the lattice parameters of the grown GaN. The value of lattice constant c for GaN layer was calculated to be 0.5178 nm. Therefore, a compressive strain is found to be present in the hetero-epitaxially grown GaN film on a-sapphire as the c value was reduced by 0.15% from the strain-free GaN (c=0.5185 nm)[20] film. This strain analysis reveals that a less lattice mismatched a-plane sapphire substrate will lead to the growth of high quality strain relaxed heteroepitaxial GaN film. The average size of the crystal was determined from the (0002) of GaN peak using the Scherrer formula[21]:

$$t = \frac{k\lambda}{\beta \cos\theta} \qquad (2)$$

where, 't' is the crystal size, 'k' is a constant, which is 0.9, 'β' is the half width of the peak, and 'θ' is the diffraction angle of the peak. The average crystal (grain) size determined by the Scherrer method is about 26.8 nm.

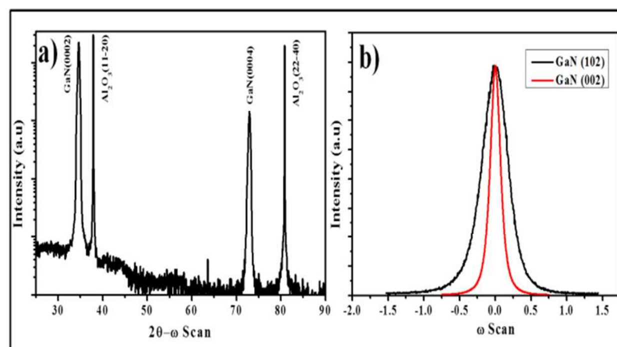

Figure 3: a) HRXRD 2-theta- omega scan of GaN film grown on a-plane sapphire (b) ω scan spectra from the symmetric (0002) and asymmetric (10-12) plane of diffraction of GaN film.

Further, HRXRD analysis has been employed to procure the information of crystalline quality as well as dislocation densities in the GaN epitaxial layer. Fig. 3 (b) shows the ω scan from the symmetric (0002) and asymmetric $(10\bar{1}2)$ plane of diffraction of GaN film having FWHM of 9.83 and 28.15 arcmin respectively. However, smaller FWHM value of symmetric scan (4 arcmin) was reported for thick (12 µm) GaN layer grown on a-plane sapphire by HVPE[22].The FWHM of the (0002) peak has been

RSC Advances Accepted Manuscript

used to evaluate the screw or mixed threading dislocation (TD) densities while the (10-12) peak is used for calculating edge TD densities. The TD density can be quantified by the following equations[21],

$$D_{Screw} = \frac{\beta^2_{(0002)}}{9b^2_{Screw}} \quad (2)$$

$$D_{Edge} = \frac{\beta^2_{(10-12)}}{9b^2_{Edge}} \quad (3)$$

Where, D_{Screw} is the screw dislocation density, D_{edge} is the edge dislocation density, β is the FWHM values measured for (0002) and $(10\bar{1}2)$ planes by HR-XRD rocking curves and b is the Burgers vector length (b_{screw}=0.5185 nm, b_{edge}=0.3189 nm). The screw and mixed dislocation densities calculated from (0002) plane of reflection is 3.3 E8 cm^{-2} while the edge dislocation densities evaluated from $(10\bar{1}2)$ plane is 7.0 E9 cm^{-2}. Therefore, these TDs are the cause of V-pits in the GaN film grown on a-plane sapphire substrate. A high value of TDs also points towards presence of non radiative recombination centres[23].

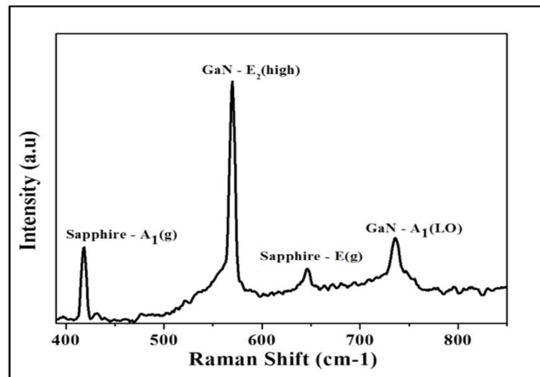

Figure 4: Room temperature Raman spectra of GaN films grown on a-plane sapphire.

As the GaN film is grown heteroepitaxially on a-plane sapphire, there will be stress generation due to difference in lattice constant of film and substrate. The developed stress in the grown GaN film is examined by Raman spectroscopy. The RT-Raman spectra is obtained in back-scattering configuration and the laser light is incident along the normal direction of the grown GaN film. Generally, E2 (High) and A1 (LO) are the only active phonon modes of GaN in this configuration at RT (Fig 4). The shift in E2 (High) phonon mode is utilized to quantify the stress/strain present in the grown film[24]. So, we prominently accentuate on the E2 (high) phonon mode peak which appeared at 569.8 cm^{-1} for the GaN film grown in this study. For stress-free GaN film, the E2 (high) mode should be visible at 567.6 cm^{-1} [25]. Thus, a blue shift of 2.2 cm^{-1} observed in the GaN film postulates that stress in the grown film is compressive in nature. Moreover, the peaks located at 735, 646 and 418 cm^{-1} belongs to the A1(LO) phonon mode of GaN, E(g) mode of sapphire and A1(g) mode of sapphire respectively. Further, the stress can be quantified by assuming a linear relationship between the E2 (high) Raman shift, Δω and the biaxial stress,

$$\sigma_{xx} : \Delta\omega = K\,\sigma_{xx} \quad (4)$$

where, K is the linear proportionality factor between the shift in the E2 (high) phonon mode and the stress. Here, we adopt a K value of 4.2 cm^{-1}/GPa[26]. The biaxial compressive stress is calculated to be 0.52 GPa in the GaN film grown by PAMBE on a-plane sapphire substrate.

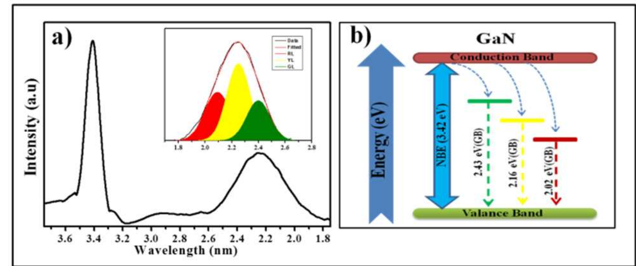

Figure 5: a) PL spectra of the grown GaN film on a-plane sapphire substrate, inset shows deconvoluted PL spectra in the range 1.7-2.8 eV at room temperature, b)) proposed schematic energy level diagram of the GaN semiconductor with various defects level state.

The detailed optical analysis of GaN film has been carried out to analyze the quality of the grown film. The room temperature PL spectrum of the grown GaN on a-plane sapphire substrate is shown in Fig 5 (a). It can be clearly seen that the radiative transition of excited electron from conduction band to valence band of GaN is at 3.41 eV. This illustrates the sharp luminescence peak of the GaN film grown on a-plane sapphire substrate where a blue shift of 10 meV observed in band-edge emission with respect to strain-free GaN (3.4 eV)[27]. The diminutive blue shifted NBE emission value is competitive to the recently enunciated stress relaxed homo-epitaxial growth of GaN film[28]. The shift in the NBE emission of GaN can be caused not only by strain but also strongly by Burstein Moss effect. The origin of shift in the NBE can be attributed to stress (0.52 GPa) present in the film, as obtained by Raman spectroscopy measurements. For an investigation of the defect generated bands in the band gap, the optical spectra in the region 1.7-2.8eV has been deconvoluted (inset Fig 5(a)) and explained. The deconvoluted spectra consist of three peaks at 2.1, 2.25 and 2.4±0.05eV which have been attributed to red luminescence (RL), yellow luminescence (YL) and green luminescence (GL) respectively. The defects related bands, like GL and RL bands are evident due to internal transitions to defects states in the GaN film by providing localized occupation to the carriers[29]. The YL band arises due to the deep acceptor levels developed caused by gallium vacancy related defects in undoped GaN[30]. A schematic representing the band diagram of the InGaN/GaN heterostructure has shown in Fig 5 (b) where the defect states and trajectory of an electron during recombination process are being depicted.

The preliminary characterisation of the epitaxial GaN film grown on a-plane sapphire substrate indicates that the film quality is appreciable. But there is a clear evidence of high density of defects related states in grown film. From the point of view of device fabrication and adopting an end to end approach, it became important to analyse how these defects states in the grown film and its influence on device performance. So the generated defects states and related recombination dynamics have been further characterised.

RSC Advances Accepted Manuscript

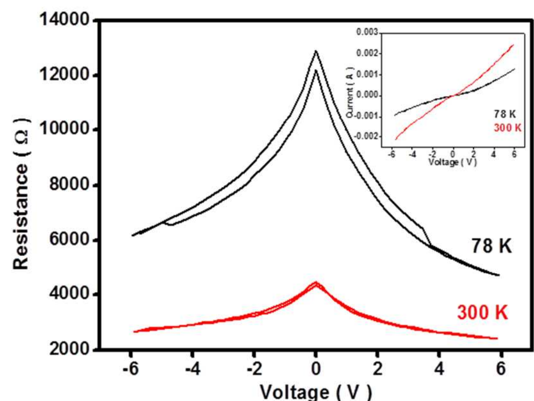

Figure 6: I-V measurements of the GaN film grown on a-plane sapphire.

I-V measurements were performed at varying temperature on the sample and a plot was obtained between the sample resistance (R) v/s the applied bias (V) (shown in inset of Fig. 6). For all practical purpose, ignoring the series resistance, the current-voltage characteristics can be represented by the equation:

$$I = Io[\exp\left(\frac{qV}{nkT}\right) - 1] \quad (5)$$

when dominated by thermionic emission with n being the ideality factor and lumping deviations from the ideal thermionic emission[31].

Where,

$$Io = AA^{*}T2\exp\left(\frac{-\phi}{kT}\right) \quad (6)$$

Here V, q, k, ϕ and T are the total applied voltage, the electron charge, the Boltzmann constant, barrier height and the absolute temperature, respectively. The contact area is A and A* is the Richardson constant. However, the plots of the I-V measurements cannot be simply fitted by the above mentioned equation for modelling ideal thermionic emission owing to bulk and surface defects. Thus, the current-voltage measurement plots deviate substantially from the aforementioned treatment and the impact of surface morphology and defects must be taken into consideration.

The temperature dependant R-V (Fig. 6) shows that there is drop in sample resistance after second voltage sweep. On consecutive voltage sweep from -6 volt to +6 volt and from +6 volt to -6 volt, we observe that the sample resistance has decreased. The magnitude of this phenomenon is found to be maximum at 0 Volt bias. In lieu of reduction of sample resistance from approximately 13 kΩ during first voltage sweep to approximately 12 kΩ during second voltage sweep it could be inferred that this reduction in resistance i.e., increase in current conduction is direct consequence of presence of deep level defects in mid- band gap region[32]. The presence of deep level defects bears an influence on the I-V characteristic with a reduced resistance at 0 Voltage in consecutive voltage sweeps due to electrons tunnelling from the Schottky barrier to an interfacial state[33]. The sample grown at 735 °C shows an improvement in its crystal quality than the sample grown at 730 °C [reported in Ref. 33]. This can be deduced from the improved current-voltage curve. The decrement in resistance in consecutive voltage sweeps is itself reduced, thus showing lesser amount of deep level defects. It is to be noted that as the quality of the film grown improves it results in elimination of such anomalies in I-V curve and results in more stable curve. Deep level defects correspond to the trap states found in forbidden band. These defects function as charge carrier trapping centres. Deep-level traps shorten the non-radiative life time of charge carriers, and through the Shockley–Read–Hall (SRH) process, thus aiding recombination of minority carriers, which has negative effects on the semiconductor device performance.

Recombination rate RT involved with traps is influenced mainly by density of trapping defects, the energy of the trapping level and the volume:

$$R_T = \frac{np - n_i^2}{\tau_{h0}(n+n_1)\tau_{e0}(p+p_1)} \quad (7)$$

Where, n and p are the concentrations of electrons and holes respectively, ni is the "intrinsic carrier concentration", and τ_{h0} and τ_{e0} are lifetime parameters (for holes and electrons respectively) whose values depend on the type of trap and the volume density of trapping defects[34]. The quantities n1 and p1 are parameters that introduce the dependency of the recombination rate on the trapping energy level Et as follows:

$$n_1 = N_c \exp\left(\frac{E_t - E_c}{kT}\right) \quad (8)$$

$$p_1 = N_v \exp\left(\frac{E_v - E_t}{kT}\right) \quad (9)$$

These expressions are of the same form as the charge carrier concentration in terms of the Fermi energy level; we can deduce from the equation that if τ_{h0} and τ_{e0} are of the same order of magnitude, for this type of recombination the maximum value will occur when the defect level lies near the middle of the forbidden band gap. Therefore, energy levels introduced by near mid gap are very effective recombination centers[32].

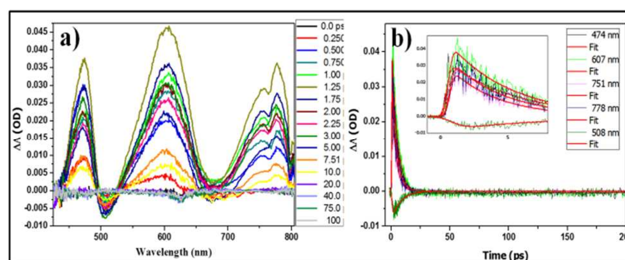

Figure 7: a) Evolution associated difference spectra of the sample excited at 320 nm for a time delay of 0-100 ps, b) The kinetic traces and their corresponding fits for a delay time of 1.25 ps at room temperature for the mentioned probe wavelengths. The inset shows the absorption signal till 8 ps for the same probe wavelengths.

To confirm the presence of defect levels in the mid-gap region ultrafast transient spectroscopy was performed in which a 320 nm pump beam was used to generate photoexcited carriers above the band-gap. The dynamics are studied by employing a white light continuum probe (1.55 to 2.92 eV). Figure 7 (a) shows the plot of differential absorption, ΔA (λ, t) (optical density) with wavelength, λ (nm) at a range of delay times, t (ps) from 0–100 ps. Three clearly distinguishable bands can be observed from a delay time of ~ 0.5 ps to 10 ps. The first two bands have peaks at ~ 474 nm (peak I) and 603 nm (peak II) and the third band is a

RSC Advances Accepted Manuscript

convolution of two peaks which are approximated at 752 nm (III a) and 777 nm (III b). On comparing the results of the photoluminescence and transient absorption data (TS), significant differences are seen in the emission and carrier relaxation[35]. It is observed that bands I, II and III b are blue shifted with respect to the PL peaks by 0.1-0.3 eV[36]. A sequential analysis of this figure reveals a maximum in ΔA (λ, t) for the three bands at a delay time of ~ 1.25ps, on either side of which the absorption decreases. This implies that around 1.25 ps all the three bands saturate and the absorption of photons by carriers in the defect levels corresponding to these three bands decreases thereafter. The positive signal disappears by ~ 20 ps indicating that the photoexcited carriers return to equilibrium. The experiment was conducted at a low fluence so as to minimize the stimulated emission. A small negative band corresponding to stimulated emission can be seen at ~ 508 nm. Figure 7 (b) illustrates the temporal decay of ΔA at saturation for fixed values of λ and the corresponding fitted curve. A multi exponential decay model with the following equation:

$$S(t) = e^{-\left(\frac{t-t_0}{IRF}\right)^2} \sum_n \left\{ A_n e^{-\left(\frac{t-t_0}{\tau_n}\right)} \right\} \quad (10)$$

is used for fitting where, IRF is instrument response time, t_0 is time zero, A_n is the percentage amplitude and τ_n is the decay time respectively. For fitting of the negative band and III (a, b) a mono-exponential decay model is used whereas for I and II a bi-exponential decay model is used. The inset clearly shows a maximal signal output at 1.25ps delay time for all probe wavelengths which is a combination of carrier thermalization time, relaxation to band-edge and the carrier localization time[37] into deep level states in the mid gap region. Neglecting the carrier thermalization time (in fs) we conclude that the carrier localization time in all the trap states is approximately same. The results obtained are in consonance with the I-V which points towards the strong presence of deep level defects in the mid–gap region. The parameters obtained from the fitting have been listed in Table 1 where, τ_1 corresponds to a non-radiative decay mechanism and τ_2 to radiative decay[38]. It illustrates that non-radiative decay mechanism is majorly responsible for the three bands and only a small part (1.32-2.11%) of ΔA is due to radiative decay[38].

Table 1: The various parameters obtained from fitting the kinetic traces at the specified probe wavelengths.

Wavelength, λ (nm)	T_0 (ps)	IRF (ps)	A_1 (%)	τ_1 (ps)	A_2 (%)	τ_2 (ps)
474.3	0.4374	0.5009	97.9	5.35	2.11	500
506.6	0.9049	1.585	100	7.62	-	-
606.9	0.5799	0.5201	98.7	4.73	1.32	500
751.1	0.6964	0.5157	100	3.57	-	-
777.8	0.6868	0.5371	100	4.04	-	-

The small lateral size of V-pits determined from figure 2 and the value of screw and edge dislocation density as evident from the calculations based on figure 3 supplements the TS, in which we see that non radiative decay is the dominant relaxation mechanism for the photo-excited carriers.

The presence of the bands can also be due to two photon absorption and its contribution cannot be ruled out. However, the parameters obtained from the fit of the kinetic traces in the TS, I-V characteristics and the photoluminescence spectrum points towards the presence of mid-gap defect levels.

4. Conclusions

We have comprehensively studied the GaN film grown on a-plane sapphire substrate to correlate via structural, optical and electrical properties with defect generated states and carriers dynamics. Morphological analysis suggests the presence of v-defects on the GaN surface. These V- pits on the GaN film are concluded to result in non-radiative carrier decay. The high density of threading dislocations results in these V-pits on the surface of single crystalline GaN film grown on a-plane sapphire substrate. From the Photoluminescence measurement it is revealed that the GaN film grown on a-plane sapphire has sharp luminescence peak and narrow NBE at 3.41 eV, and a broad defect band emission centered at 2.2 eV. The presence of deep level defects in mid- band gap region has been confirmed by variation in low temperature I-V measurements. The transient spectroscopic analysis depicts that non-radiative decay mechanism is majorly responsible from these defect states. The results clearly indicate that the film quality of GaN grown on a-plane sapphire is appreciable but with presence of some deep level defects. Such defects can be removed by investigating different growth windows. a-plane sapphire substrate shows promising results to be investigated further as an efficient substrate for growing high quality GaN film.

Acknowledgment

The authors would like to acknowledge Director, CSIR-NPL, New Delhi for his everlasting encouragement and support. The authors would also like to thank Mrs. Mandeep Kaur for FE-SEM measurements. This work is financially supported by PSC-0109 (CSIR-12th FYP). One of the authors (Shibin Krishna TC) also acknowledges Department of Science & Technology (DST), India and Simco Global Technology & Systems Ltd. for financial assistance under the Prestigious Prime Minister Doctoral Fellowship.

References:

1. K. Chung, C. H. Lee, and G. C. Yi, Science, **330**, 655 (2010).
2. J. Wu, J. Appl. Phys. **106**, 011101 (2009).
3. L. Liu and J. H. Edgar, Mater. Sci. Eng. R 37, 61 (2002).
4. S. C. Jain, M. Willander, and J. Narayan, J. Appl. Phys. **87**, 965 (2000).
5. T. Matsuoka, T. Sakai, and A. Katsui, Opteletronics Devices and Technologies. **5**, 53 (1990).
6. T. D. Moustakas, R. J. Molnar, T. Lei, G. Menon, and C. R. Eddy, Jr. Mater. Res. Soc. Symp. Proc. **242**, 427 (1992).
7. T. D. Moustakas, T. Lei and R. J. Molnar, Physica B **185**, 36 (1993).
8. K. Doverspike, L. B. Rowland, D. K. Gaskill, and J. A. Freitas, Jr., J. Electron. Mater. **24**, 269 (1994).

RSC Advances Accepted Manuscript

9. T. Y. Lin, G. M. Chen, D. Y. Lyu, Solid State Communication. **142**, 237, (2007).
10. Y. Y. Wong, E. Y. Chang, T. H. Yang, J. R. Chang, J. T. Ku, M. K. Hudait, W. C. Chou, M. Chen, and K. L. Lin, J. Electrochem. Soc., **157**, H746 (2010).
11. D. Doppalapudi, E. Iliopoulos, S. N. Basu, and T. D. Moustakas, J. Appl. Phys., **85**, 3582 (1999).
12. K. H Baik, J.Kim, J. Ceram. Pro. Res., **8**, 277 (2007).
13. S. K. Hong, T. Yao, B. J. Kim, S. Y. Yoon, T. I. Kim, Appl. Phys. Lett. **77**, 82 (2000).
14. Be're´ and A. Serra, Phys. Rev. B **65** (20), 205 (2002).
15. D. Won, X. Weng, and J. M. Redwing, J. Appl. Phys. **108**(9), 093511 (2010).
16. Y. Chen, T. Takeuchi, H. Amano, I. Akasaki, N. Yamada, Y. Kaneko, and S. Y. Wang, Appl. Phys. Lett. **72**, 710 (1998).
17. H. Kim, H. S. Park, Y. J. Park, and T. Kim, Appl. Phys. Lett. **73**, 1634 (1998).
18. N. Sharma, P. Thomas, D. Tricker, and C. Humphreys, Appl. Phys. Lett. **77**, 1274 (2000).
19. J. Kim, Y. H. Cho, D. S. Ko, X. S. Li, J. Y. Won, E. Lee, S. H. Park, J. Y. Kim, and S. Kim, Opt. Exp. **22**, A857 (2014).
20. C. Boney, I. Hernandez, R. Pillai, D. Starikov, A. Bensaoula, M. Henini, M. Syperek, J. Misiewicz, Kudrawiec, R. Phys. Stat. Sol. (c). **8**, 2466 (2011).
21. M. A. Moram and M. E. Vickers in Rep. Prog. Phys. **72**, 036502 (2009).
22. T. Paskova, E. B Svedberg, A. Henry, I. G. Ivanov, R. Yakimova, and B. Monemar, Physica Scr. **79**, 67 (1999).
23. T. Sugahara, H. Sato, M. Hao, Y. Naoi, S. Kurai, S. Tottori, K. Yamashita, K. Nishino, L. T. Romano and S. S. Sugahara, Jpn. J. Appl. Phys. **37**, L398 (1998).
24. Z. C. Feng, W. Wang, S. J. Chua, P. X. Zhang, K. P. J. Williams and G. D. Pitt, J. Raman Spt. 32, 840 (2001).
25. A. R. Goñi, H. Siegle, K. Syassen, C. Thomsen, and J.-M. Wagner, Phys. Rev. B **64**, 035205 (2001).
26. C. Kisielowski, J. Krüger, S. Ruvimov, T. Suski, J. W. Ager, III, E. Jones, Z. Liliental-Weber, M. Rubin, E. R. Weber, M. D. Bremser, and R. F. Davis, Phys. Rev. B **54**, 17745 (1996).
27. S. Strite, H. J. Morkoc, J. Vac. Sci. Technol. *B.* **10**, 1237 (1992).
28. N. Aggarwal, S. Krishna TC, L. Goswami, M. Mishra, G. Gupta, K. K. Mau rya, S. Singh, N. Dilawar, M. Kaur, Cryst. Grow. Des. **15**, 2144 (2015).
29. M. A. Reshchikov, H. Morkoc, J. Appl. Phys. **97**, 061301 (2005).
30. J. Neugebauer, C. G. Van de Walle, Appl. Phys. Lett. **69**, 503 (1996).
31. K. Shiojima and T. Suemitsu, J. Vac. Sci. Technol. B **21**, 698 (2003).
32. H. Markoc, *Handbook of Nitride Semiconductors and Devices* (Vol-**2**, Wiley-VCH, Chapter 1, 2008).
33. A. G. Reddy, N. Aggarwal, S.Krishna TC, M. Singh, R. Rakshit, and G. Gupta Appl. Phys. Lett. **106**, 233501 (2015).
34. M. A. Green, *Solar Cells: Operating Principles, Technology, and System Applications* (Englewood Cliffs: Prentice-Hall, Inc., 1982).
35. A. Othonos, G. Itskos, D. D. C. Bradley, M. D. Dawson and I. M. Watson, Appl. Phys. Lett. 94, 203102 (2009).
36. D.M. Hofmann, B.K. Meyer, H. Alves, F. Leiter, W. Burkhard, N. Romanov, Y. Kim, J. Krüger and E.R. Weber, Phys. Stat. Sol (b) 180, 261 (2000).
37. G. Bing, W. K. Sing, Y. Z. Zhen, J. H. Xing and L. J. Yu, Chinese Phys. Lett. **20**, 749 (2003).
38. H. Haag, B. Hönerlage, O. Briot, and R. L. Aulombard, Phys. Rev. B **60**, 11624 (1999).

RSC Advances Accepted Manuscript